CMS Physics Analysis Summary

Contact: cms-phys-conveners-ftr@cern.ch 2019/01/24

Search for supersymmetry with direct stau production at the HL-LHC with the CMS Phase-2 detector

The CMS Collaboration

Abstract

A search for the direct production of τ sleptons ($\widetilde{\tau}$) is developed assuming 3000 fb^{-1} of proton-proton collision data produced by the HL-LHC at a center-of-mass energy of 14 TeV. Three final states are investigated: two τ leptons decaying hadronically, and one τ lepton decaying hadronically and the other one decaying to a muon or electron and neutrinos. The analysis is performed using the Delphes simulation of the CMS Phase-2 detector where the object reconstruction performance is tuned to the one achieved with CMS Phase-2 full simulation. In the mass-degenerate production scenario, $\widetilde{\tau}$ masses are excluded below 650 GeV, with the discovery contour of $\widetilde{\tau}$ masses reaching up to 470 GeV.

This document has been revised with respect to the version dated November 11, 2018.

1 Introduction

Supersymmetry (SUSY) [1–8] is an attractive extension of the standard model (SM) of particle physics. It potentially provides solutions to some of the shortcomings affecting the SM, such as the need for fine tuning [9–14] to explain the observed value of the Higgs boson mass [15–20], and the absence of a dark matter (DM) candidate. Supersymmetric models are characterized by the presence of a superpartner for every SM particle with the same quantum numbers except that its spin differs from that of its SM counterpart by half a unit. The cancellation of quadratic divergences in quantum corrections to the Higgs boson mass from SM particles and their superpartners could resolve the fine-tuning problem. In SUSY models with R-parity conservation [21], the lightest supersymmetric particle (LSP) is stable [22, 23] and could be a DM candidate [24]. The superpartners of the electroweak gauge and Higgs bosons, namely the bino, winos, and Higgsinos, mix to form neutral and charged mass eigenstates, referred to as the neutralinos ($\widetilde{\chi}_i^0$) and charginos ($\widetilde{\chi}_i^{\pm}$), respectively. Here we assume $\widetilde{\chi}_1^0$, the lightest neutralino, to be the LSP.

The analysis reported in this note investigates the production of the hypothetical τ slepton (stau, denoted by $\widetilde{\tau}$), the superpartner of the τ lepton. Supersymmetric scenarios in which the $\widetilde{\tau}$ is light, lead to final states with one or more τ leptons. Coannihilation scenarios, characterized by a light $\widetilde{\tau}$ that has a small mass splitting with an almost pure bino-like LSP, lead to a DM relic density consistent with cosmological observations [25–30], making the search for new physics in these final states particularly interesting. In this analysis, we examine simplified SUSY models [31–34] in which the $\widetilde{\tau}$ can be produced directly through pair production and decays to a τ lepton and the LSP. The most sensitive searches for direct $\widetilde{\tau}$ pair production to date were performed at the CERN LEP collider [35–39]. At the CERN LHC, the ATLAS [40, 41] and CMS [42, 43] Collaborations have both performed searches for direct and indirect $\widetilde{\tau}$ production with 8 TeV LHC data. CMS has also investigated $\widetilde{\tau}$ production with 13 TeV data [44].

In many SUSY scenarios the $\widetilde{\tau}$ mass is lighter than the one of selectrons and smuons. The large data set expected at the HL-LHC provides an unprecedented opportunity to probe for the direct production of $\widetilde{\tau}$, which is a challenge due to the relatively small production cross section. For example, the cross section in the mass-degenerate scenario, where we assume that the left- and right-handed $\widetilde{\tau}$ have the same mass and add up their cross sections, for a $\widetilde{\tau}$ mass of 100 GeV is 0.41 pb, and for 300 GeV it is reduced to 0.0071 pb, while for a $\widetilde{\tau}$ mass of 500 GeV we expect only a cross section of 0.79 fb [45]. A search is therefore developed in events where both τ leptons decay either hadronically ("$\tau_h\tau_h$" analysis), and in events where one of the τ leptons decays hadronically (denoted in the following by τ_h) and the other one to a muon or electron and neutrinos ("$\ell\tau_h$" analysis).

The simplified model used for the optimization of the search and the interpretation of the results is shown in Fig. 1. The search assumes $\widetilde{\tau}$ pair production in the mass-degenerate scenario. The cross sections have been computed for $\sqrt{s} = 14$ TeV at next-to-leading order (NLO) using the Prospino code [46]. Final values are calculated using the PDF4LHC recommendations for the two sets of cross sections following the prescriptions of the LHC SUSY Cross Section Working Group [45]. The branching ratio of the $\widetilde{\tau}$ into the τ lepton and the $\widetilde{\chi}_1^0$ is assumed to be 100%.

2 The upgraded CMS detector

The CMS detector [47] will be substantially upgraded in order to fully exploit the physics potential offered by the increase in luminosity at the HL-LHC [48], and to cope with the demand-

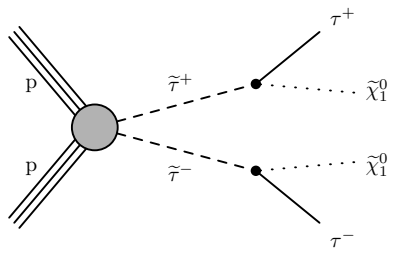

Figure 1: Diagram for the $\widetilde{\tau}$ pair production.

ing operational conditions at the HL-LHC [49–53]. The upgrade of the first level hardware trigger (L1) will allow for an increase of L1 rate and latency to about 750 kHz and 12.5 μs, respectively, and the high-level software trigger (HLT) is expected to reduce the rate by about a factor of 100 to 7.5 kHz. The entire pixel and strip tracker detectors will be replaced to increase the granularity, reduce the material budget in the tracking volume, improve the radiation hardness, and extend the geometrical coverage and provide efficient tracking up to pseudorapidities of about $|\eta| = 4$. The muon system will be enhanced by upgrading the electronics of the existing cathode strip chambers (CSC), resistive plate chambers (RPC) and drift tubes (DT). New muon detectors based on improved RPC and gas electron multiplier (GEM) technologies will be installed to add redundancy, increase the geometrical coverage up to about $|\eta| = 2.8$, and improve the trigger and reconstruction performance in the forward region. The barrel electromagnetic calorimeter (ECAL) will feature the upgraded front-end electronics that will be able to exploit the information from single crystals at the L1 trigger level, to accommodate trigger latency and bandwidth requirements, and to provide 160 MHz sampling allowing high precision timing capability for photons. The hadronic calorimeter (HCAL), consisting in the barrel region of brass absorber plates and plastic scintillator layers, will be read out by silicon photomultipliers (SiPMs). The endcap electromagnetic and hadron calorimeters will be replaced with a new combined sampling calorimeter (HGCal) that will provide highly segmented spatial information in both transverse and longitudinal directions, as well as high-precision timing information. Finally, the addition of a new timing detector for minimum ionizing particles (MTD) in both barrel and endcap region is envisaged to provide capability for 4-dimensional reconstruction of interaction vertices that will allow to significantly offset the CMS performance degradation due to high PU rates.

A detailed overview of the CMS detector upgrade program is presented in Ref. [49–53], while the expected performance of the reconstruction algorithms and the mitigation of pileup, i.e., additional proton-proton collisions within the same or neighboring bunch crossings, is summarized in Ref. [54].

3 Object reconstruction and simulated samples

The event reconstruction uses a particle-flow (PF) algorithm [55], combining information from the tracker, calorimeter, and muon systems to identify charged and neutral hadrons, photons, electrons, and muons in an event. Candidate events are expected to contain at least two leptons: either two τ_h candidates, or one τ_h and one muon or electron from τ lepton decays. In order to pass the selection, electrons (muons) are required to have a transverse momentum $p_T > 30$ GeV and pseudorapidity $|\eta| < 1.6(2.4)$. Dedicated lepton identification criteria are applied, providing 50% to 90% efficiency for muons and 25% to 80% efficiency for electrons, depending on the lepton p_T and η. Both muons and electrons are required to be isolated. The

isolation is calculated from the scalar sum of the p_T of all particles within a cone of radius $R = \sqrt{(\Delta\eta)^2 + (\Delta\phi)^2} = 0.3$ around the lepton momentum vector, excluding the contribution of the lepton and applying an area-based correction to remove the contribution of particles from pileup [56]. The ratio I_{rel} of the scalar sum of the p_T in the cone to the transverse momentum of the lepton itself is required to be smaller than 0.05.

Jets are reconstructed using the anti-k_T algorithm [57, 58], with a distance parameter of 0.4. For this study we use PUPPI jets [59] which are required to have $p_T > 30\,\text{GeV}$ and $|\eta| < 2.7$. Jets originating from b quarks are identified with the loose working point of the combined secondary vertex b tagging algorithm (CSVv2) [60], which corresponds to an efficiency of about 60–65%.

The τ_h candidates must satisfy $p_T > 40\,\text{GeV}$ in the $\ell\tau_h$ final states, while a slightly higher threshold of $p_T > 50\,\text{GeV}$ is required for the $\tau_h\tau_h$ final state, driven by the trigger thresholds foreseen for the HL-LHC. Since the main background in this analysis is due to events with jets misidentified as τ_h leptons, a tight working point with a small misidentification rate is chosen for τ_h identification. The τ_h reconstruction efficiency for this working point is about 30%, with a misidentification rate of about 0.08% assuming a multivariate analysis optimization. Overlaps between the two reconstructed leptons in the $\ell\tau_h$ final state are avoided by requiring them to have a minimum separation in ΔR of 0.3.

In order to ensure orthogonality between the different final states and suppress background, we reject events with additional electrons or muons beyond the two selected leptons that satisfy slightly less stringent selection criteria and transverse momentum of $p_T > 20\,\text{GeV}$ and $|\eta| < 2.7$.

The object selection requirements implemented in the analysis are summarized in Table 1.

Table 1: Summary of object selection requirements for the analysis.

Selection requirement	$\ell\tau_h$	$\tau_h\tau_h$
Muon (electron) p_T	$> 30\,\text{GeV}$	—
Muon (electron) p_T (veto)	$> 30\,\text{GeV}$	$> 20\,\text{GeV}$
Muon (electron) $\|\eta\|$	$< 2.4(1.6)$	—
Muon (electron) $\|\eta\|$ (veto)	< 2.7	< 2.7
τ_h p_T	$> 40\,\text{GeV}$	$> 50\,\text{GeV}$
τ_h $\|\eta\|$	< 2.3	< 2.3
p_T (τ_h τ_h)	—	$> 50\,\text{GeV}$
jet p_T (veto)	$> 30\,\text{GeV}$	$> 30\,\text{GeV}$
jet $\|\eta\|$ (veto)	< 2.7	< 2.7
b jet p_T (veto)	$> 20\,\text{GeV}$	$> 30\,\text{GeV}$

The MADGRAPH5_aMC@NLO 2.3.3 generator [61] is used to produce the parton-level background processes at leading order (LO), with the parton showering and hadronization provided by PYTHIA 8.212 [62, 63]. Signal models of direct $\widetilde{\tau}$ pair production are generated with MADGRAPH5_aMC@NLO at LO precision in perturbative quantum chromodynamics (QCD) up to the production of τ leptons, which are then decayed with PYTHIA 8.212. The NNPDF3.0LO set of parton distribution functions is used in the generation of all signal models.

The potential effect of pileup is estimated by overlaying the hard scatter event with minimum bias events drawn from a Poisson distribution with a mean of 200.

The generated signal and background events are processed with the fast-simulation package Delphes [64] in order to simulate the expected response of the upgraded CMS detector. The

object reconstruction and identification efficiencies, as well as the detector response and resolution, are parameterized in Delphes using the detailed simulation of the upgraded CMS detector based on GEANT4 package [65, 66].

The detailed simulation of the upgraded CMS detector and objects performance at HL-LHC include the effects of aging in the barrel calorimeter that correspond to an integrated luminosity of 1000 fb^{-1}.

4 Event selection

The event selection for each final state requires the presence of exactly two reconstructed leptons with opposite charges, corresponding to the $\tau_h\tau_h$ or $\ell\tau_h$ final states. In order to suppress backgrounds with top quarks, we veto events containing any b-tagged jet in both final states. For the $\ell\tau_h$ analysis, the p_T threshold for b-tagged jets is lowered to 20 GeV, as this allows to significantly reduce the background from W+jets events, where the W boson decays into an electron or muon and a neutrino, and a jet is misidentified as τ_h.

The main background for the $\tau_h\tau_h$ final state after this selection consists of QCD multijet events, W+jets, DY+jets, and top quark events. Separating the background into prompt τ_h events, where both reconstructed τ leptons are matched to a generator τ_h, and misidentified events, where one or more non-generator matched jets have been misidentified as prompt τ_h, we find that the misidentified background dominates our search regions.

In the $\ell\tau_h$ final state, all events with at least one jet are rejected. Due to kinematical constraints in the signal, we reduce the background from QCD multijet events by requiring a maximum separation of the two leptons in ΔR of 3.5.

The baseline selection criteria described above are summarized in Table 2. The baseline events are then further selected using kinematic variables for each of the three final states to improve the sensitivity of the search to a range of sparticle masses.

Table 2: Summary of the baseline selection requirements in each final state.

Selection requirement	$\ell\tau_h$	$\tau_h\tau_h$
$\Delta\phi(\ell_1, \ell_2)$	> 1.5	> 1.5
$\Delta R(\ell_1, \ell_2)$	$0.3 < \Delta R < 3.5$	—
Veto of events with b-tagged jets	yes	yes
N_{jet}	$= 0$	—

In order to further improve discrimination against the SM background, we take advantage of the expected presence of two $\widetilde{\chi}_1^0$ in the final state for signal events, which would lead to missing transverse momentum, $\vec{p}_T^{\,\text{miss}}$. The missing transverse momentum vector $\vec{p}_T^{\,\text{miss}}$ is defined as the negative vector sum of all PF candidates with corresponding transverse momenta weighted through the PUPPI method. Its magnitude is referred to as p_T^{miss}.

In addition, mass observables that can be calculated from the reconstructed leptons and the $\vec{p}_T^{\,\text{miss}}$ provide strong discriminants between signal and background. For a mother particle decaying to a visible and an invisible particle, the transverse mass M_T has a kinematic endpoint at the mass of the mother particle, and is calculated as follows:

$$M_T(\ell, \vec{p}_T^{\,\text{miss}}) \equiv \sqrt{2 p_\ell p_T^{\text{miss}} (1 - \cos\Delta\phi(\vec{p}_\ell, \vec{p}_T^{\,\text{miss}}))}. \quad (1)$$

In addition, the scalar sum of the M_{T} calculated with the first and second lepton and the missing transverse momentum, respectively, is used to further reduce the background events: $\Sigma M_{\mathrm{T}} = M_{\mathrm{T}}(\ell_1, \vec{p}_{\mathrm{T}}^{\,\mathrm{miss}}) + M_{\mathrm{T}}(\ell_2, \vec{p}_{\mathrm{T}}^{\,\mathrm{miss}})$.

We also calculate the stransverse mass M_{T2} [67, 68], defined as:

$$M_{\mathrm{T2}}(m_s, \vec{s}, m_t, \vec{t}, \vec{p}_{\mathrm{T}}^{\,\mathrm{miss}}; \chi_1, \chi_2) = \min_{\substack{\vec{p},\vec{q}\ \text{s.t.} \\ \vec{p}+\vec{q}=\vec{p}_{\mathrm{T}}^{\,\mathrm{miss}}}} \left\{ \max\left[M_{\mathrm{T}}(m_s, \vec{s}, \chi_1, \vec{p}), M_{\mathrm{T}}(m_t, \vec{t}, \chi_2, \vec{q}) \right] \right\} \quad (2)$$

where the transverse mass is given by

$$M_{\mathrm{T}}(m, \vec{v}, \chi, \vec{p}) = \sqrt{m^2 + \chi^2 + 2\sqrt{m^2 + |\vec{v}|^2}\sqrt{\chi^2 + |\vec{p}|^2} - 2\vec{v}\cdot\vec{p}},$$

in which $\vec{s}$, $\vec{t}$, $\vec{p}$, $\vec{q}$, and $\vec{p}_{\mathrm{T}}^{\,\mathrm{miss}}$ are all real two-vectors, and the remaining quantities are real scalars which may all be assumed to be nonnegative as they only enter through their squares. As input for the visible particles ($\vec{s}$ and $\vec{t}$) we give the four-vectors of the two leptons, and we define the mass of the invisible particles $\chi_1 = \chi_2 = 0$. The M_{T2} requirement reduces background from diboson production.

4.1 Search regions for the $\tau_{\mathrm{h}}\tau_{\mathrm{h}}$ analysis

The main variables that are used to define the search regions are ΣM_{T} and M_{T2}, which are shown for the baseline selection in Fig. 2. All processes containing top quarks, i.e., $\mathrm{t\bar{t}}$, single top quark, and $\mathrm{t\bar{t}}$ +X production are combined and referred to "Top Quark" in the figure, while "Other SM" corresponds to background processes with low cross section that are combined, namely diboson and triboson production.

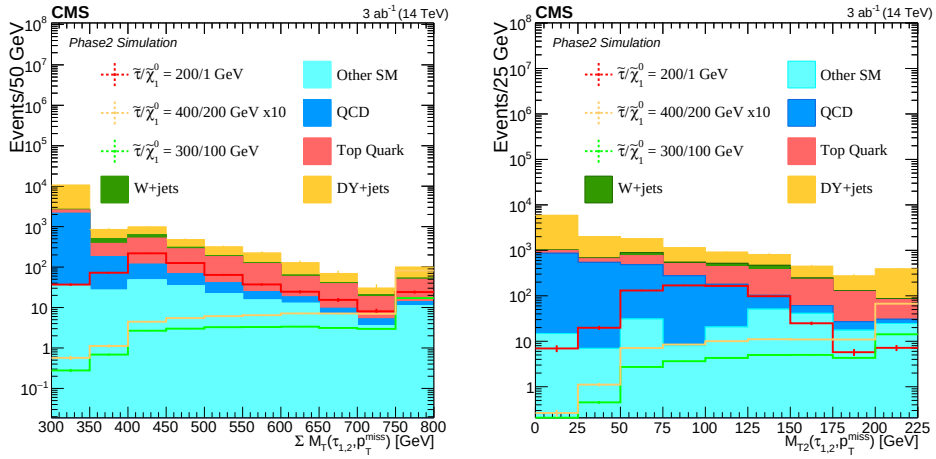

Figure 2: The main search variables for the $\tau_{\mathrm{h}}\tau_{\mathrm{h}}$ analysis, (left) ΣM_{T} and (right) M_{T2}, both after the baseline selection. Scaled signal yields for direct $\tilde{\tau}$ production with the mass-degenerate cross section are shown for three separate scenarios of $\tilde{\tau}$ and LSP masses. All processes containing top quarks, i.e. $\mathrm{t\bar{t}}$, single top quark, and $\mathrm{t\bar{t}}$ +X production are combined and referred to "Top Quark" in the figure, while "Other SM" corresponds to background processes with a low number of events that are combined, diboson and triboson production.

While we apply a stringent requirement of at least 400 GeV for ΣM_{T}, we require M_{T2} to be above 50 GeV.

The search regions, binned in M_{T2}, ΣM_T, and the number of jets n_{jet}, are summarized in Table 3. There are 24 regions in total.

Table 3: Definition of the search regions (SR) used in the $\tau_h\tau_h$ analysis. Signal depleted bins (low ΣM_T, high M_{T2}) are omitted. The full list of bins and background yields is presented in Table 6.

Variable	Bin 0	Bin 1	Bin 2	Bin 3
M_{T2}	$50 < M_{T2} < 100\,\text{GeV}$	$100 < M_{T2} < 150\,\text{GeV}$	$150 < M_{T2} < 200\,\text{GeV}$	$M_{T2} > 200\,\text{GeV}$
ΣM_T	$400 < \Sigma M_T < 500\,\text{GeV}$	$500 < \Sigma M_T < 600\,\text{GeV}$	$\Sigma M_T > 600\,\text{GeV}$	—
n_{jet}	$= 0$	> 0	—	—

4.2 Search regions for the $\ell\tau_h$ analysis

In the $\ell\tau_h$ final state, we require $M_T(\ell, \vec{p}_T^{\,miss}) > 120\,\text{GeV}$, which reduces the W+jets background significantly. To further suppress the SM background in the leptonic final states, we require p_T^{miss} to be at least 150 GeV, which mainly reduces QCD multijets and Drell-Yan events. Additional requirements on M_{T2} and the τ_h p_T are applied to define the search regions, as summarized in Table 4. Figures 3 and 4 show the distributions of M_{T2}, M_T, and M_{T2} before the signal region selection for the $e\tau_h$ and $\mu\tau_h$ channel, respectively. In these figures, the "Other SM" refers to processes with a low number of events after the baseline selection and includes diboson, triboson, $t\bar{t}$ and single top production.

Table 4: Search region requirements in the $\ell\tau_h$ analysis.

Variable	Bin 0	Bin 1	Bin 2	Bin 3
M_{T2}	$M_{T2} > 120\,\text{GeV}$	$M_{T2} > 120\,\text{GeV}$	$80 < M_{T2} < 120\,\text{GeV}$	$80 < M_{T2} < 120\,\text{GeV}$
$p_T(\tau_h)$	$> 200\,\text{GeV}$	$40 < p_T(\tau_h) < 200\,\text{GeV}$	$> 200\,\text{GeV}$	$40 < p_T(\tau_h) < 120\,\text{GeV}$

5 Systematic uncertainties

The dominant experimental uncertainties are those originating from jets being misidentified as τ_h, the lepton efficiency, the jet energy scale and resolution, b tagging efficiency and integrated luminosity. These systematic uncertainties are correlated between the signal and the irreducible background yields. The sources of the systematic uncertainties and their values are reported in Table 5.

6 Results

The expected yields in the $\tau_h\tau_h$ final state after all selection requirements are given in Table 6.

The expected yields for the $e\tau_h$ and the $\mu\tau_h$ analysis are given in Tables 7 and 8, respectively, for all signal regions.

The expected upper limits at the 95% confidence level (CL), calculated using the asymptotic formulae [69] of the CL_s criterion [70, 71], and the 5σ discovery potential are given in Fig. 5. The $\tau_h\tau_h$ analysis has been found to drive the sensitivity, but adding the $\ell\tau_h$ channel enlarges the exclusion bounds by about 60–80 GeV.

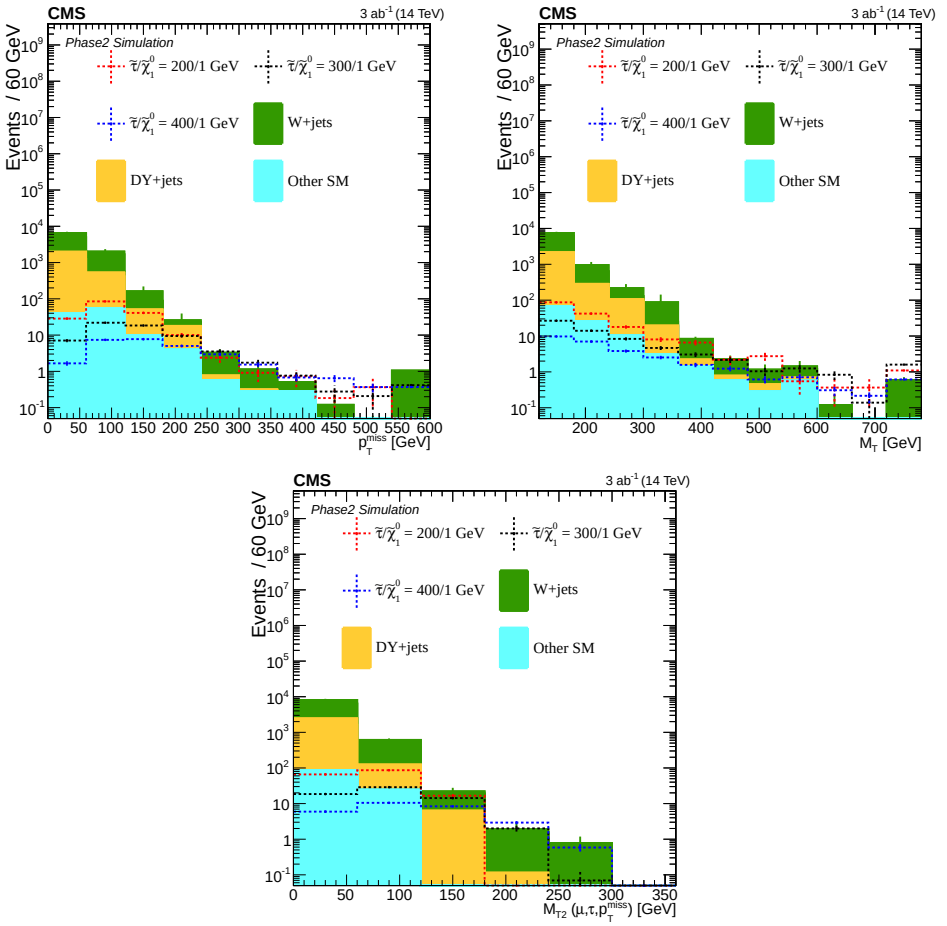

Figure 3: The variables used to determine the search regions in the eτ_h analysis after the baseline selection: (upper left) the p_T^{miss} distribution, (upper right) the M_T distribution, and (lower) the M_{T2} distribution using p_T^{miss} after the baseline selection. "Other SM" refers to processes with a low number of events after the baseline selection and includes diboson, triboson, $t\bar{t}$ and single top quark production.

Table 5: Summary of the experimental systematic uncertainties.

Source of systematic uncertainty	Value
τ_h efficiency	2.5%
τ_h misidentification rate	15%
Muon efficiency	0.5%
Electron efficiency	1%
Jet energy scale	1–3.5%
Jet energy resolution	3–5%
b tagging	1%
Integrated luminosity	1%

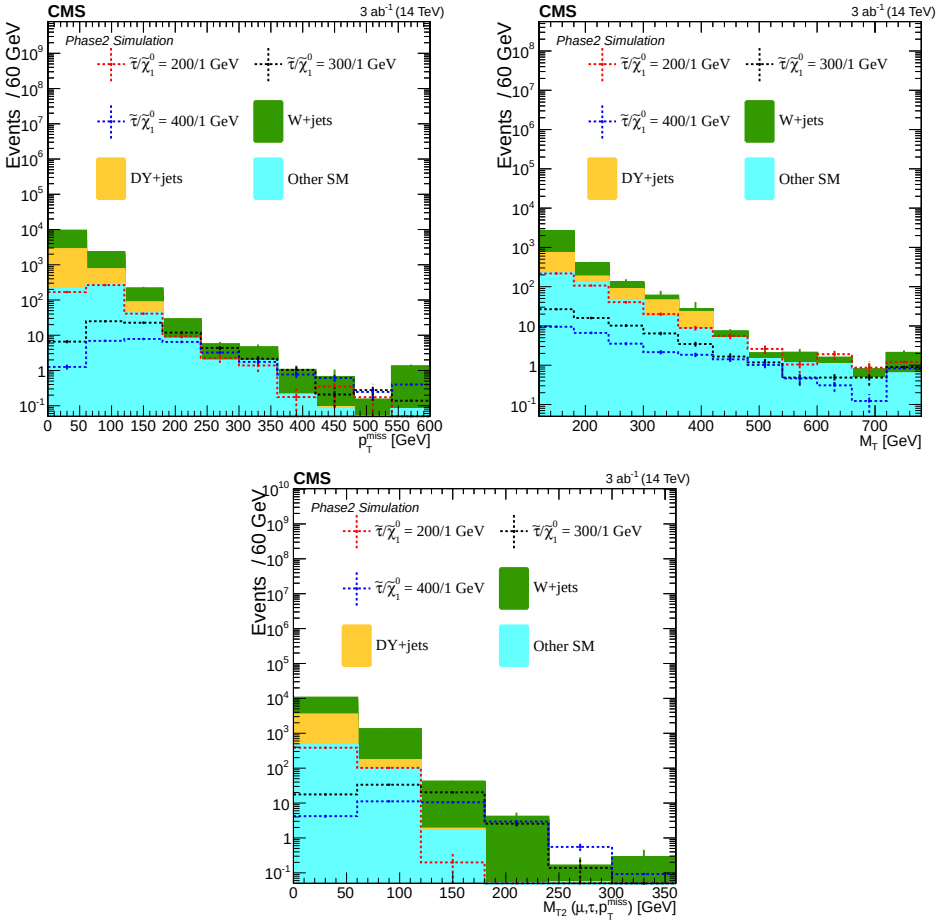

Figure 4: The variables used to determine the search regions in the $\mu\tau_h$ analysis after the baseline selection: (upper left) the p_T^{miss} distribution, (upper right) the M_T distribution, and (lower) the M_{T2} distribution using p_T^{miss} after the baseline selection. "Other SM" refers to processes with a low number of events after the baseline selection and includes diboson, triboson, $t\bar{t}$ and single top quark production.

Table 6: Signal region yields for for background and signal simulation in the $\tau_h\tau_h$ channel. The three rightmost columns show the signal predictions in the degenerate scenario, for masses given in the form of $(m_{\tilde{\tau}}/m_{\tilde{\chi}_1^0})$ in GeV.

Bin	DY+jets	W+jets	$t\bar{t}$	QCD	Other SM	Sum	(200/100)	(500/200)	(700/300)
SR-$\tau_h\tau_h$-M_{T2}_0_M_T_0_N_j_0	79.67 ± 32.14	58.80 ± 43.95	13.21 ± 3.86	5.41 ± 0.17	2.92 ± 2.35	160.00 ± 54.63	104.79 ± 4.62	1.19 ± 0.05	0.22 ± 0.01
SR-$\tau_h\tau_h$-M_{T2}_0_M_T_0_N_j_1	57.76 ± 15.39	5.07 ± 0.52	104.54 ± 11.30	28.19 ± 0.33	8.78 ± 2.62	204.33 ± 19.28	56.96 ± 3.40	0.79 ± 0.04	0.16 ± 0.01
SR-$\tau_h\tau_h$-M_{T2}_0_M_T_1_N_j_0	9.86 ± 6.28	3.96 ± 0.29	4.53 ± 2.24	1.26 ± 0.09	3.70 ± 1.54	23.31 ± 6.85	26.51 ± 2.32	0.72 ± 0.04	0.17 ± 0.01
SR-$\tau_h\tau_h$-M_{T2}_0_M_T_1_N_j_1	1.36 ± 0.06	1.33 ± 0.13	31.25 ± 6.01	3.84 ± 0.11	2.79 ± 1.54	40.57 ± 6.21	18.99 ± 1.96	0.62 ± 0.04	0.14 ± 0.01
SR-$\tau_h\tau_h$-M_{T2}_0_M_T_2_N_j_0	0.51 ± 0.04	2.85 ± 0.25	2.61 ± 1.79	0.38 ± 0.05	-	6.35 ± 1.81	21.82 ± 2.11	1.33 ± 0.06	0.40 ± 0.02
SR-$\tau_h\tau_h$-M_{T2}_0_M_T_2_N_j_1	9.69 ± 6.28	0.86 ± 0.10	26.11 ± 5.56	0.86 ± 0.03	2.77 ± 1.54	40.28 ± 8.53	15.32 ± 1.76	1.11 ± 0.05	0.35 ± 0.02
SR-$\tau_h\tau_h$-M_{T2}_1_M_T_0_N_j_0	32.60 ± 11.17	6.15 ± 0.53	16.36 ± 4.32	2.89 ± 0.18	4.99 ± 1.85	62.98 ± 12.13	83.71 ± 4.13	1.14 ± 0.05	0.19 ± 0.01
SR-$\tau_h\tau_h$-M_{T2}_1_M_T_0_N_j_1	2.03 ± 0.10	1.34 ± 0.25	66.90 ± 8.74	18.17 ± 0.33	1.44 ± 1.62	89.89 ± 8.90	40.00 ± 2.84	0.74 ± 0.04	0.13 ± 0.01
SR-$\tau_h\tau_h$-M_{T2}_1_M_T_1_N_j_0	19.59 ± 9.63	1.14 ± 0.20	3.96 ± 2.19	1.52 ± 0.11	0.56 ± 0.89	26.78 ± 9.92	25.73 ± 2.29	1.26 ± 0.05	0.25 ± 0.01
SR-$\tau_h\tau_h$-M_{T2}_1_M_T_1_N_j_1	0.47 ± 0.05	0.56 ± 0.44	13.32 ± 3.91	5.19 ± 0.15	2.70 ± 1.36	22.24 ± 4.17	12.93 ± 1.62	0.91 ± 0.05	0.16 ± 0.01
SR-$\tau_h\tau_h$-M_{T2}_1_M_T_2_N_j_0	9.08 ± 6.28	0.28 ± 0.06	0.05 ± 0.01	0.68 ± 0.07	2.11 ± 1.03	12.20 ± 6.37	10.83 ± 1.48	2.13 ± 0.07	0.57 ± 0.02
SR-$\tau_h\tau_h$-M_{T2}_1_M_T_2_N_j_1	3.79 ± 2.51	0.06 ± 0.02	5.65 ± 2.53	1.37 ± 0.06	1.18 ± 1.03	12.05 ± 3.71	9.03 ± 1.35	1.78 ± 0.06	0.57 ± 0.02
SR-$\tau_h\tau_h$-M_{T2}_2_M_T_1_N_j_0	0.17 ± 0.03	0.32 ± 0.10	0.05 ± 0.01	0.55 ± 0.08	1.03 ± 0.73	2.12 ± 0.74	2.69 ± 0.73	0.63 ± 0.04	0.11 ± 0.01
SR-$\tau_h\tau_h$-M_{T2}_2_M_T_1_N_j_1	3.73 ± 2.51	0.22 ± 0.07	8.71 ± 3.13	1.84 ± 0.11	1.06 ± 0.73	15.57 ± 4.08	1.71 ± 0.58	0.39 ± 0.03	0.07 ± 0.01
SR-$\tau_h\tau_h$-M_{T2}_2_M_T_2_N_j_0	0.23 ± 0.04	0.17 ± 0.05	0.04 ± 0.01	0.73 ± 0.07	0.02 ± 0.73	1.18 ± 0.73	2.48 ± 0.71	2.95 ± 0.08	0.80 ± 0.02
SR-$\tau_h\tau_h$-M_{T2}_2_M_T_2_N_j_1	0.19 ± 0.02	0.04 ± 0.01	5.59 ± 2.53	1.51 ± 0.07	0.06 ± 0.73	7.38 ± 2.64	1.52 ± 0.54	2.19 ± 0.07	0.67 ± 0.02
SR-$\tau_h\tau_c dh$-M_{T2}_3_M_T_2_N_j_0	53.02 ± 30.56	0.03 ± 0.02	0.02 ± 0.00	0.27 ± 0.03	0.03 ± 0.02	53.36 ± 30.56	0.24 ± 0.20	3.61 ± 0.09	1.74 ± 0.04
SR-$\tau_h\tau_h$-M_{T2}_3_M_T_2_N_j_1	0.06 ± 0.01	0.02 ± 0.01	2.52 ± 1.59	0.50 ± 0.03	0.54 ± 0.51	3.66 ± 1.67	0.90 ± 0.41	3.17 ± 0.09	1.72 ± 0.04

Table 7: Signal region yields for background and signal simulation in the $e\tau_h$ channel. The three rightmost columns show the signal predictions in the degenerate scenario, for masses given in the form of $(m_{\tilde{\tau}}/m_{\tilde{\chi}_1^0})$ in GeV.

SR name	DY	W+Jets	Other SM	Sum	(200/1)	(300/1)	(400/1)
SR-eτ_h_1	0.18 ± 0.07	6.83 ± 1.45	0.03 ± 0.06	7.03 ± 1.45	3.13 ± 0.78	6.83 ± 0.71	2.54 ± 0.24
SR-eτ_h_2	0.44 ± 0.11	10.06 ± 1.52	0.98 ± 0.13	11.00 ± 1.53	8.60 ± 1.30	7.42 ± 0.74	2.36 ± 0.23
SR-eτ_h_3	0.15 ± 0.06	10.11 ± 1.41	0.62 ± 0.10	10.57 ± 1.41	5.86 ± 1.07	3.71 ± 0.52	1.30 ± 0.17
SR-eτ_h_4	0.10 ± 0.05	3.42 ± 0.87	0.38 ± 0.08	4.31 ± 0.97	4.10 ± 0.90	2.60 ± 0.44	0.58 ± 0.11

Table 8: Signal region yields for background and signal simulation in the $\mu\tau_h$ channel. The three rightmost columns show the signal predictions in the degenerate scenario, for masses given in the form of $(m_{\tilde{\tau}}/m_{\tilde{\chi}_1^0})$ in GeV.

SR name	DY	W+Jets	Other SM	Sum	(200/1)	(300/1)	(400/1)
SR-$\mu\tau_h$_0	0.06 ± 0.02	7.82 ± 1.27	0.12 ± 0.13	7.94 ± 1.28	4.57 ± 0.91	9.50 ± 0.81	7.14 ± 0.47
SR-$\mu\tau_h$_1	0.13 ± 0.04	20.51 ± 2.11	0.76 ± 0.29	21.62 ± 2.16	7.49 ± 1.17	9.43 ± 0.81	5.02 ± 0.39
SR-$\mu\tau_h$_2	0.07 ± 0.03	12.02 ± 1.65	0.72 ± 0.19	12.53 ± 1.66	6.76 ± 1.11	6.03 ± 0.65	2.68 ± 0.29
SR-$\mu\tau_h$_3	0.03 ± 0.02	3.19 ± 0.74	1.88 ± 0.31	4.86 ± 0.87	4.38 ± 0.89	1.25 ± 0.29	0.68 ± 0.14

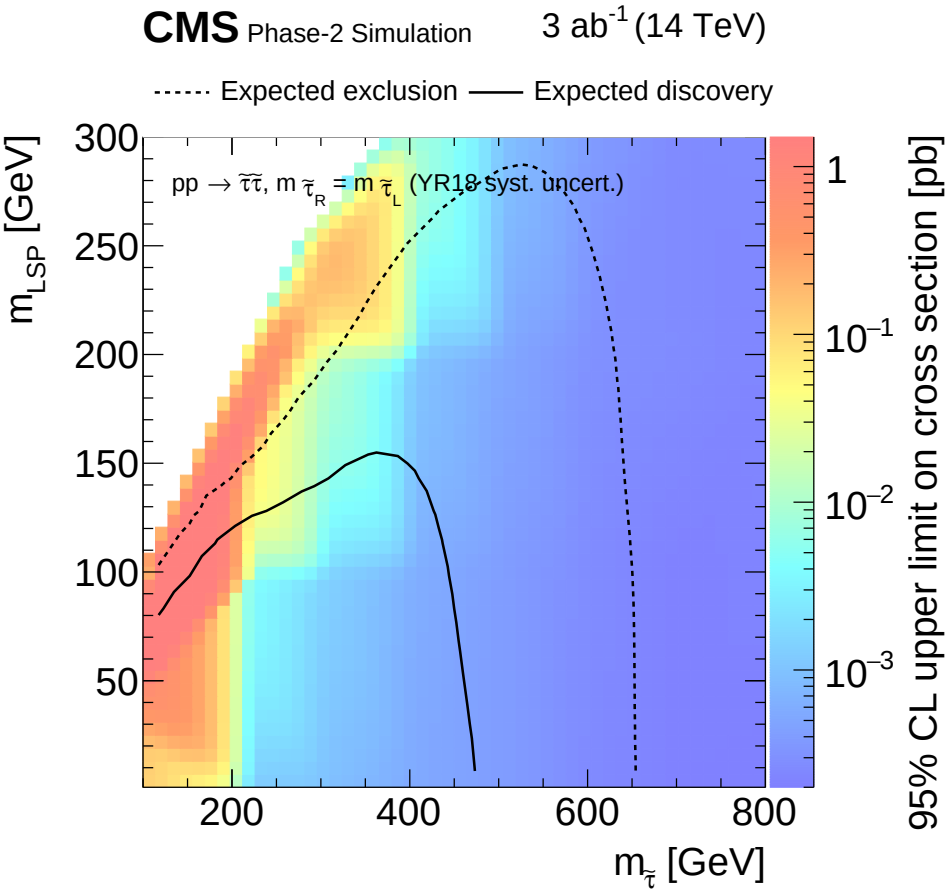

Figure 5: The expected upper limits at the 95% CL and the 5σ discovery potential for the combination of the results of the $\tau_h\tau_h$ and $\ell\tau_h$ channels.

7 Summary

A search for the direct production of τ sleptons has been presented, assuming 3000 fb^{-1} of proton-proton collision data produced by the HL-LHC at a center-of-mass energy of 14 TeV. Expected limits have been calculated for the final states that contain either two hadronically decaying τ leptons and missing transverse momentum, or one hadronically decaying τ lepton and one τ decaying to a muon or electron and neutrinos. The analysis is performed using the Delphes simulation of the CMS Phase-2 detector where the object reconstruction performance is tuned to the one achieved with CMS Phase-2 full simulation. In mass-degenerate scenarios, degenerate production of τ sleptons are excluded up to 650 GeV with the discovery contour reaching up to 470 GeV for a massless lightest neutralino.

References

[1] P. Ramond, "Dual theory for free fermions", *Phys. Rev. D* **3** (1971) 2415, doi:10.1103/PhysRevD.3.2415.

[2] Y. A. Gol'fand and E. P. Likhtman, "Extension of the algebra of Poincaré group generators and violation of P invariance", *JETP Lett.* **13** (1971) 323.

[3] A. Neveu and J. H. Schwarz, "Factorizable dual model of pions", *Nucl. Phys. B* **31** (1971) 86, doi:10.1016/0550-3213(71)90448-2.

[4] D. V. Volkov and V. P. Akulov, "Possible universal neutrino interaction", *JETP Lett.* **16** (1972) 438.

[5] J. Wess and B. Zumino, "A Lagrangian model invariant under supergauge transformations", *Phys. Lett. B* **49** (1974) 52, doi:10.1016/0370-2693(74)90578-4.

[6] J. Wess and B. Zumino, "Supergauge transformations in four dimensions", *Nucl. Phys. B* **70** (1974) 39, doi:10.1016/0550-3213(74)90355-1.

[7] P. Fayet, "Supergauge invariant extension of the Higgs mechanism and a model for the electron and its neutrino", *Nucl. Phys. B* **90** (1975) 104, doi:10.1016/0550-3213(75)90636-7.

[8] H. P. Nilles, "Supersymmetry, supergravity and particle physics", *Phys. Rep.* **110** (1984) 1, doi:10.1016/0370-1573(84)90008-5.

[9] G. 't Hooft, "Naturalness, chiral symmetry, and spontaneous chiral symmetry breaking", *NATO Sci. Ser. B* **59** (1980) 135.

[10] E. Witten, "Dynamical breaking of supersymmetry", *Nucl. Phys. B* **188** (1981) 513, doi:10.1016/0550-3213(81)90006-7.

[11] M. Dine, W. Fischler, and M. Srednicki, "Supersymmetric technicolor", *Nucl. Phys. B* **189** (1981) 575, doi:10.1016/0550-3213(81)90582-4.

[12] S. Dimopoulos and S. Raby, "Supercolor", *Nucl. Phys. B* **192** (1981) 353, doi:10.1016/0550-3213(81)90430-2.

[13] S. Dimopoulos and H. Georgi, "Softly broken supersymmetry and SU(5)", *Nucl. Phys. B* **193** (1981) 150, doi:10.1016/0550-3213(81)90522-8.

[14] R. K. Kaul and P. Majumdar, "Cancellation of quadratically divergent mass corrections in globally supersymmetric spontaneously broken gauge theories", *Nucl. Phys. B* **199** (1982) 36, doi:10.1016/0550-3213(82)90565-X.

[15] ATLAS Collaboration, "Observation of a new particle in the search for the standard model Higgs boson with the ATLAS detector at the LHC", *Phys. Lett. B* **716** (2012) 1, doi:10.1016/j.physletb.2012.08.020, arXiv:1207.7214.

[16] CMS Collaboration, "Observation of a new boson at a mass of 125 GeV with the CMS experiment at the LHC", *Phys. Lett. B* **716** (2012) 30, doi:10.1016/j.physletb.2012.08.021, arXiv:1207.7235.

[17] CMS Collaboration, "Observation of a new boson with mass near 125 GeV in pp collisions at $\sqrt{s}$ = 7 and 8 TeV", *JHEP* **06** (2013) 081, doi:10.1007/JHEP06(2013)081, arXiv:1303.4571.

[18] ATLAS Collaboration, "Measurement of the Higgs boson mass from the $H \to \gamma\gamma$ and $H \to ZZ^* \to 4\ell$ channels with the ATLAS detector using 25 fb^{-1} of pp collision data", *Phys. Rev. D* **90** (2014) 052004, doi:10.1103/PhysRevD.90.052004, arXiv:1406.3827.

[19] CMS Collaboration, "Precise determination of the mass of the Higgs boson and tests of compatibility of its couplings with the standard model predictions using proton collisions at 7 and 8 TeV", *Eur. Phys. J. C* **75** (2015) 212, doi:10.1140/epjc/s10052-015-3351-7, arXiv:1412.8662.

[20] ATLAS and CMS Collaborations, "Combined measurement of the Higgs boson mass in pp collisions at $\sqrt{s} = 7$ and 8 TeV with the ATLAS and CMS experiments", *Phys. Rev. Lett.* **114** (2015) 191803, doi:10.1103/PhysRevLett.114.191803, arXiv:1503.07589.

[21] G. R. Farrar and P. Fayet, "Phenomenology of the production, decay, and detection of new hadronic states associated with supersymmetry", *Phys. Lett. B* **76** (1978) 575, doi:10.1016/0370-2693(78)90858-4.

[22] C. Boehm, A. Djouadi, and M. Drees, "Light scalar top quarks and supersymmetric dark matter", *Phys. Rev. D* **62** (2000) 035012, doi:10.1103/PhysRevD.62.035012, arXiv:hep-ph/9911496.

[23] C. Balázs, M. Carena, and C. E. M. Wagner, "Dark matter, light stops and electroweak baryogenesis", *Phys. Rev. D* **70** (2004) 015007, doi:10.1103/PhysRevD.70.015007, arXiv:hep-ph/403224.

[24] G. Jungman, M. Kamionkowski, and K. Griest, "Supersymmetric dark matter", *Phys. Rept.* **267** (1996) 195, doi:10.1016/0370-1573(95)00058-5, arXiv:hep-ph/9506380.

[25] G. Hinshaw et al., "Nine-year Wilkinson Microwave Anisotropy Probe (WMAP) observations: cosmological parameter results", *Astrophys. J. Suppl.* **208** (2013) 19, doi:10.1088/0067-0049/208/2/19, arXiv:1212.5226.

[26] K. Griest and D. Seckel, "Three exceptions in the calculation of relic abundances", *Phys. Rev. D* **43** (1991) 3191, doi:10.1103/PhysRevD.43.3191.

[27] D. A. Vasquez, G. Belanger, and C. Boehm, "Revisiting light neutralino scenarios in the MSSM", *Phys. Rev. D* **84** (2011) 095015, doi:10.1103/PhysRevD.84.095015, arXiv:1108.1338.

[28] S. F. King, J. P. Roberts, and D. P. Roy, "Natural dark matter in SUSY GUTs with non-universal gaugino masses", *JHEP* **10** (2007) 106, doi:10.1088/1126-6708/2007/10/106, arXiv:0705.4219.

[29] M. Battaglia et al., "Proposed post-LEP benchmarks for supersymmetry", *Eur. Phys. J. C* **22** (2001) 535, doi:10.1007/s100520100792, arXiv:hep-ph/0106204.

[30] R. L. Arnowitt et al., "Determining the dark matter relic density in the mSUGRA (x0(1))- tau co-annhiliation region at the LHC", *Phys. Rev. Lett.* **100** (2008) 231802, doi:10.1103/PhysRevLett.100.231802, arXiv:0802.2968.

[31] CMS Collaboration, "Interpretation of searches for supersymmetry with simplified models", *Phys. Rev. D* **88** (2013) 052017, doi:10.1103/PhysRevD.88.052017, arXiv:1301.2175.

[32] J. Alwall, P. Schuster, and N. Toro, "Simplified models for a first characterization of new physics at the LHC", *Phys. Rev. D* **79** (2009) 075020, doi:10.1103/PhysRevD.79.075020.

[33] J. Alwall, M.-P. Le, M. Lisanti, and J. Wacker, "Model-independent jets plus missing energy searches", *Phys. Rev. D* **79** (2009) 015005, doi:10.1103/PhysRevD.79.015005.

[34] LHC New Physics Working Group, "Simplified models for LHC new physics searches", *J. Phys. G* **39** (2012) 105005, doi:10.1088/0954-3899/39/10/105005, arXiv:1105.2838.

[35] ALEPH Collaboration, "Search for scalar leptons in e^+e^- collisions at center-of-mass energies up to 209 GeV", *Phys. Lett. B* **526** (2002) 206, doi:10.1016/S0370-2693(01)01494-0, arXiv:hep-ex/0112011.

[36] DELPHI Collaboration, "Searches for supersymmetric particles in e^+e^- collisions up to 208 GeV and interpretation of the results within the MSSM", *Eur. Phys. J. C* **31** (2003) 421, doi:10.1140/epjc/s2003-01355-5, arXiv:hep-ex/0311019.

[37] L3 Collaboration, "Search for scalar leptons and scalar quarks at LEP", *Phys. Lett. B* **580** (2004) 37, doi:10.1016/j.physletb.2003.10.010, arXiv:hep-ex/0310007.

[38] OPAL Collaboration, "Search for anomalous production of dilepton events with missing transverse momentum in e^+e^- collisions at $\sqrt{s}$ = 183 GeV to 209 GeV", *Eur. Phys. J. C* **32** (2004) 453, doi:10.1140/epjc/s2003-01466-y, arXiv:hep-ex/0309014.

[39] LEP SUSY Working Group (ALEPH, DELPHI, L3, OPAL), "Combined LEP selectron/smuon/stau results, 183-208 GeV", (2004). LEPSUSYWG/04-01.1.

[40] ATLAS Collaboration, "Search for the direct production of charginos, neutralinos and staus in final states with at least two hadronically decaying taus and missing transverse momentum in pp collisions at $\sqrt{s}$ = 8 TeV with the ATLAS detector", *JHEP* **10** (2014) 96, doi:10.1007/JHEP10(2014)096, arXiv:1407.0350.

[41] ATLAS Collaboration, "Search for the electroweak production of supersymmetric particles in $\sqrt{s} = 8$ TeV pp collisions with the ATLAS detector", *Phys. Rev. D* **93** (2016) 052002, doi:10.1103/PhysRevD.93.052002, arXiv:1509.07152.

[42] CMS Collaboration, "Search for electroweak production of charginos in final states with two tau leptons in pp collisions at $\sqrt{s} = 8$ TeV", *JHEP* **04** (2017) 018, doi:10.1007/JHEP04(2017)018, arXiv:1610.04870.

[43] CMS Collaboration, "Search for supersymmetry in the vector-boson fusion topology in proton-proton collisions at $\sqrt{s} = 8$ TeV", *JHEP* **11** (2015) 189, doi:10.1007/JHEP11(2015)189, arXiv:1508.07628.

[44] CMS Collaboration, "Search for supersymmetry in events with a τ lepton pair and missing transverse momentum in proton-proton collisions at $\sqrt{s} = 13$ TeV", arXiv:1807.02048.

[45] B. Fuks, M. Klasen, D. R. Lamprea, and M. Rothering, "Revisiting slepton pair production at the Large Hadron Collider", *JHEP* **01** (2014) 168, doi:10.1007/JHEP01(2014)168, arXiv:1310.2621.

[46] W. Beenakker, R. Hopker, and M. Spira, "PROSPINO: A Program for the production of supersymmetric particles in next-to-leading order QCD", arXiv:hep-ph/9611232.

[47] CMS Collaboration, "The CMS Experiment at the CERN LHC", *JINST* **3** (2008) S08004, doi:10.1088/1748-0221/3/08/S08004.

[48] G. Apollinari et al., "High-Luminosity Large Hadron Collider (HL-LHC) : Preliminary Design Report", doi:10.5170/CERN-2015-005.

[49] D. Contardo et al., "Technical Proposal for the Phase-II Upgrade of the CMS Detector",.

[50] K. Klein, "The Phase-2 Upgrade of the CMS Tracker",.

[51] C. Collaboration, "The Phase-2 Upgrade of the CMS Barrel Calorimeters Technical Design Report", Technical Report CERN-LHCC-2017-011. CMS-TDR-015, CERN, Geneva, Sep, 2017. This is the final version, approved by the LHCC.

[52] C. Collaboration, "The Phase-2 Upgrade of the CMS Endcap Calorimeter", Technical Report CERN-LHCC-2017-023. CMS-TDR-019, CERN, Geneva, Nov, 2017. Technical Design Report of the endcap calorimeter for the Phase-2 upgrade of the CMS experiment, in view of the HL-LHC run.

[53] C. Collaboration, "The Phase-2 Upgrade of the CMS Muon Detectors", Technical Report CERN-LHCC-2017-012. CMS-TDR-016, CERN, Geneva, Sep, 2017. This is the final version, approved by the LHCC.

[54] CMS Collaboration, "CMS Phase 2 object performance", Technical Report CMS-PAS-FTR-18-012, in preparation.

[55] CMS Collaboration, "Particle-flow reconstruction and global event description with the CMS detector", *JINST* **12** (2017) P10003, doi:10.1088/1748-0221/12/10/P10003, arXiv:1706.04965.

[56] M. Cacciari and G. P. Salam, "Pileup subtraction using jet areas", *Phys. Lett. B* **659** (2008) 119, doi:10.1016/j.physletb.2007.09.077, arXiv:0707.1378.

[57] M. Cacciari, G. P. Salam, and G. Soyez, "The anti-k_{T} jet clustering algorithm", *JHEP* **04** (2008) 063, doi:10.1088/1126-6708/2008/04/063, arXiv:0802.1189.

[58] M. Cacciari, G. P. Salam, and G. Soyez, "FastJet user manual", *Eur. Phys. J. C* **72** (2012) 1896, doi:10.1140/epjc/s10052-012-1896-2, arXiv:1111.6097.

[59] D. Bertolini, P. Harris, M. Low, and N. Tran, "Pileup Per Particle Identification", *JHEP* **10** (2014) 059, doi:10.1007/JHEP10(2014)059, arXiv:1407.6013.

[60] CMS Collaboration, "Identification of heavy-flavour jets with the CMS detector in pp collisions at 13 TeV", (2017). arXiv:1712.07158. Submitted to *JINST*.

[61] J. Alwall et al., "The automated computation of tree-level and next-to-leading order differential cross sections, and their matching to parton shower simulations", *JHEP* **07** (2014) 079, doi:10.1007/JHEP07(2014)079, arXiv:1405.0301.

[62] T. Sjöstrand, S. Mrenna, and P. Z. Skands, "A Brief Introduction to PYTHIA 8.1", *Comput. Phys. Commun.* **178** (2008) 852, doi:10.1016/j.cpc.2008.01.036, arXiv:0710.3820.

[63] T. Sjostand and *al*, "AnintroductiontoPYTHIA8.2", *Comput.Phys.Commun.* **191** (2015) doi:doi:10.1016/j.cpc.2015.01.024, arXiv:1410.3012.

[64] DELPHES 3 Collaboration, "DELPHES 3, A modular framework for fast simulation of a generic collider experiment", *JHEP* **02** (2014) 057, doi:10.1007/JHEP02(2014)057, arXiv:1307.6346.

[65] GEANT4 Collaboration, "GEANT4: A Simulation toolkit", *Nucl. Instrum. Meth.* **A 506** (2003) 250, doi:10.1016/S0168-9002(03)01368-8.

[66] J. Allison et al., "Geant4 developments and applications", *IEEE Trans. Nucl. Sci.* **53** (2006) 270, doi:10.1109/TNS.2006.869826.

[67] C. G. Lester and D. J. Summers, "Measuring masses of semiinvisibly decaying particles pair produced at hadron colliders", *Phys. Lett. B* **463** (1999) 99, doi:10.1016/S0370-2693(99)00945-4, arXiv:hep-ph/9906349.

[68] A. Barr, C. Lester, and P. Stephens, "m_{T2}: the truth behind the glamour", *J. Phys. G* **29** (2003) 2343, doi:10.1088/0954-3899/29/10/304, arXiv:hep-ph/0304226.

[69] G. Cowan, K. Cranmer, E. Gross, and O. Vitells, "Asymptotic formulae for likelihood-based tests of new physics", *Eur. Phys. J. C* **71** (2011) 1554, doi:10.1140/epjc/s10052-011-1554-0, arXiv:1007.1727. [Erratum: doi:10.1140/epjc/s10052-013-2501-z].

[70] T. Junk, "Confidence level computation for combining searches with small statistics", *Nucl. Instrum. Meth. A* **434** (1999) 435, doi:10.1016/S0168-9002(99)00498-2, arXiv:hep-ex/9902006.

[71] A. L. Read, "Presentation of search results: the CL_s technique", *J. Phys. G* **28** (2002) 2693, doi:10.1088/0954-3899/28/10/313.